Error modelling and validation of a high-precision five degree of freedom hybrid mechanism for high-power high-repetition rate laser operations

Shah Karim[1], Samanta Piano[1], Richard Leach[1], Martin Tolley[2]

[1]Manufacturing Metrology Team, Faculty of Engineering, University of Nottingham, Nottingham, NG7 2RD, UK

[2]Central Laser Facility, Science and Technologies Facilities Council, Oxfordshire, OX11 0QX, UK

Abstract. The accuracy, repeatability and speed requirements of high-power laser operations demand the employment of five degree of freedom motion control solutions that are capable of positioning and orientating the target with respect to the laser(s)-target interaction point with high accuracy and precision. The combined serial and parallel kinematic (hybrid) mechanism reported in this paper is a suitable candidate for this purpose; however, a number of error sources can affect its performance. A kinematic model to analyse the errors causing the positional and orientational deviations of the target is described considering two rotational degrees of freedom of the hybrid mechanism. Strategies are outlined to simplify the error analysis and to determine the error parameters of the mechanism using the error model and an experimental technique.

Keywords degree of freedom, hybrid mechanism, parallel kinematic structure, RPS mechanism, generalised error parameters, parasitic motion, error model.

1. Introduction

Pulsed lasers with high power (petawatt class lasers) have seen significant development in the last few decades. High-power lasers are used for advanced research activities in physics, chemistry and biology, for example, to accelerate subatomic particles to high energies, to study biochemical and biophysical processes, and for cutting-edge applications, such as fusion energy, radiation therapy and secondary source generation (X-rays, electrons, protons, neutron and ions) [1-3]. To utilise the full potential of high-power lasers, large-scale facilities need to

operate at high-repetition rates, which presents many engineering challenges [3,4]. One such challenge is the positioning and aligning of a micro-scale target (or in short 'target') relative to the focus of the laser beam(s) with an accuracy of few micrometres - a fundamental requirement for a high-power laser-target interaction to ensure that targets are reproducibly accessible to the highest intensities available, that is in the region of the laser beam focus as determined by the Rayleigh range [5,6]. Fulfilling this requirement for a high-repetition rate laser system means that new targets have to be positioned and aligned at the laser beam focus at a rate of at least 0.1 Hz (with plans for 10 Hz or higher in future) [4-6]. To meet the specifications for target positioning accuracy and to achieve the required speed of high-repetition rate laser operations, the Central Laser Facility (CLF) has designed and developed a new high-accuracy microtargetry system (HAMS) for mounting and motion control of targets for the Astra-Gemini high-power laser [7,8].

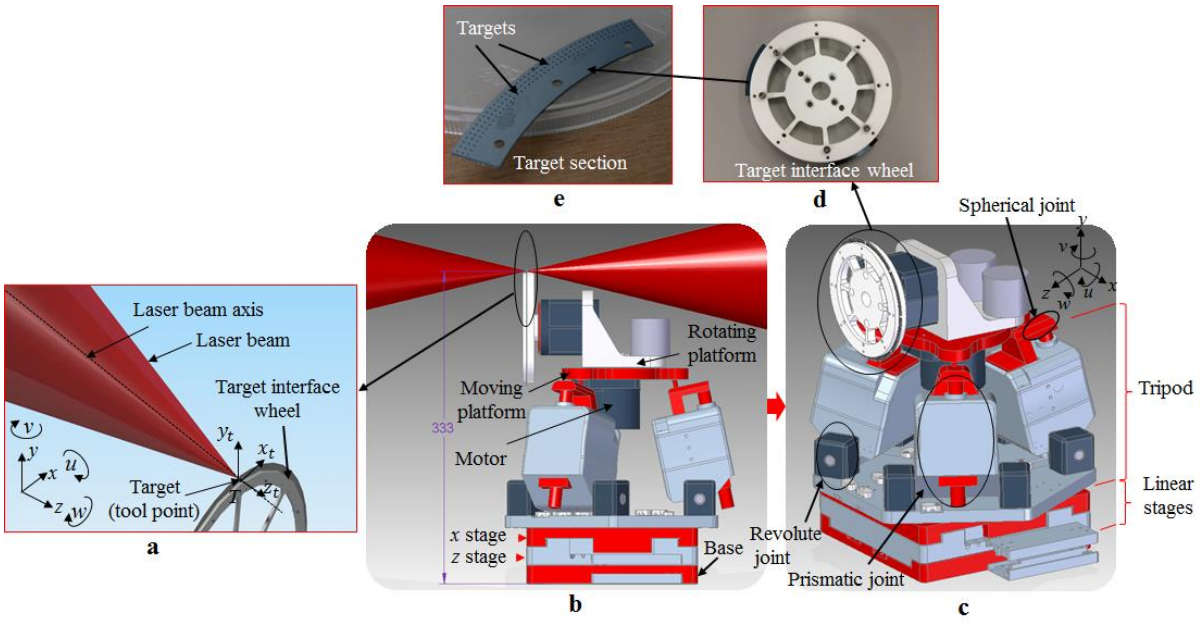

Figure 1. HAMS for the high power high repetition rate laser operations: (a) laser beam-target interaction; (b) HAMS with the target interface wheel; (c) features of HAMS; (d) target interface wheel with two target sections; (e) targets patterned around the circumference of a target section (adapted from [4] and [8]).

HAMS is based on a tripod architecture mounted on a two-axis linear stage, providing control of all five degrees of freedom for positioning and aligning a target at the laser beam focus (Figure 1*a*-*c*). Therefore, HAMS has a hybrid kinematic structure, comprising parallel and serial mechanisms. A hybrid structure is usually designed to

overcome the inherent limitations of serial and parallel mechanisms, such as low accuracy and limited workspace, respectively, while exploiting the advantageous characteristics of both types, namely large workspace and high accuracy [9,10]. An application, for example, requiring high-accuracy motion over a relatively large workspace can use a hybrid structure as an effective solution. Tricept and Exechon are examples of two commercially available hybrid machine tools [11,12]. Although hybrid structures have recently received much attention, and research is underway on how to use them in industrial applications, comprehensive studies of their design, kinematics, dynamics and error sources are lacking [12].

In addition to a tripod and a two-axis linear stage, HAMS has an interface wheel to which target sections, made using micro-electro-mechanical system (MEMS) techniques and typically from a silicon wafer, are attached, and a number of different target sizes/designs are patterned around the circumference of the section (see Figure 1*c*-*e*). The ability of HAMS to provide positioning and alignment accuracy of the target within the defined specification is dependent upon a number of factors, such as the target geometry, accumulation of errors on the motion stages and the tripod (rotational and translational motion errors, orthogonality errors, wobble/eccentricity errors, etc.), and the flatness tolerances on the wafer and interface wheel [6-8]. Many of these factors are examples of geometric errors, which can arise from the physical errors, such as manufacturing and assembling errors of the components of a mechanism, and joint errors of a mechanism. These geometric errors can affect the performance of a hybrid mechanism, just like any other precision machine and, therefore, error compensation is required to minimise the positional deviations at the target during the target alignment process [13,14]. Effective error compensation strategies for high-precision applications depend on identifying the sources of geometric error [15] and, as such, developing an error model based on kinematic analysis of the mechanism is essential for this purpose [15,16].

Developing an error model for a hybrid mechanism can be challenging for a number of reasons, particularly [17]:

- The error sources associated with serial kinematic mechanisms have been widely studied and are well understood [17-20], while those associated with parallel mechanisms are less well understood.
- Due to their relatively simpler kinematics, error analysis of serial mechanisms is mostly carried out following direct kinematic analysis, which determines a set of input joint variables to achieve a known pose (position

and orientation) of the end-effector [12]. However, parallel mechanisms generally have more complex kinematics, and pursuing a direct kinematic analysis may be difficult.

- In all parallel mechanisms, various types of geometric error can be related to some physical errors, particularly machining and assembly errors of the mechanism, such as platform frame errors, pin joint errors and spherical joint assembly errors. Theoretical analysis to understand the effects of all these physical errors can be a complex and lengthy process. Although some studies have been pursued to understand the effects of the significant geometric errors of some parallel mechanisms [15,21], in most cases, the actual effects of the errors on the final position of the target remain unclear, since it is assumed that some error averaging effects take place for the parallel mechanisms as opposed to the cumulative addition of errors for the serial mechanisms.

In this paper, the development of a kinematic model for a particular type of hybrid mechanism HAMS is presented, with an analysis of the error sources and experimental validation to demonstrate how the errors may affect the positioning and orientation accuracy of targets during the CLF's target alignment process of the laser operations. Through the development of an error model for HAMS, this paper shows that a practical strategy to develop an error model for a hybrid mechanism should simplify the kinematic analysis of the mechanism. This is achieved by considering (a) the errors that may have significant effects on the particular motion/s of the mechanism, (b) the "generalised" errors, which can sufficiently describe the deviations of the geometric properties of a kinematic system in a mechanism, instead of considering all possible individual sources of geometric errors of that system, (c) the angular errors that can potentially be amplified by the structural offsets to produce significant translational errors at the target, and (d) the strategy of measuring the errors to estimate their effects on the positional accuracy of the target.

2. Motions of HAMS

In the HAMS hybrid mechanism, two translation motions (along *x* and *z* axes, see Figure 1*b*-*c*) are generated from a linear *xz* system, which is a two degree of freedom (DOF) serial mechanism. The tripod, the parallel part of the hybrid mechanism, provides a rotational motion about the *x* axis (called tip *u*) and a translational motion along the *y* axis, while the rotary motor, which actuates the rotating platform mounted on the moving platform of the tripod,

produces a further rotational motion about the *y* axis (called tilt *v*) (Figure 1*a*-*c*). The moving platform of the tripod and the rotating platform can be considered as serially connected, jointly having three degrees of freedom. Since the linear *xz* system is widely used in industry and the technology is well developed, this research has focused on the error analysis of the parallel part (tripod) and its serially connected rotating platform. Note that an additional rotary motion (about the *z* axis) is required to rotate the target wheel, but this motion is not related to the tripod, rotating platform or linear *xz* system.

With regard to the 3 DOF platform (that is, moving and rotating as shown in Figure 1*b*-*c*), only the tip and tilt motions are considered for the kinematic analysis of this paper. This is because tip and tilt motions control the orientation of the target on the target interface wheel. The optimal location of a target is primarily determined by the z_t direction (see Figure 1*a*), which is usually along the laser axis. Therefore, the z_t direction is considered as the most sensitive direction for the target alignment. Typically, the target alignment method of the CLF suggests that the target needs to be orientated to the laser beam by controlling the tip and tilt motions of HAMS, followed by the position adjustments of the target in the *x*, *z* and/or *y* directions by controlling the linear motions of the *xz* system and/or the vertical motion of the tripod, respectively. However, point to note that the order of the angular motions (tip and tilt or tilt and tip) has effect on the final position of the target. The choice of the order to follow depends on the requirements of the application to which the mechanism is being used, and the structure of the mechanism.

3. Kinematic analysis of HAMS

3.1 Kinematic structure of HAMS

From a mechanism viewpoint, the tripod can be described as a RPS system, where *R*, *P* and *S* denote revolute joint, prismatic joint (linear slider) and spherical joint respectively. In a RPS system, one end of each of the three actuated prismatic joints (legs) is attached to a non-actuated revolute joint, while the other end of the leg is fixed to the moving platform with a non-actuated spherical joint (Figure 1*b*-*c*) [22].

Figure 2 schematically represents the kinematic structure of HAMS, describing the geometrical relationships among the coordinate systems placed at the points of interest for the analysis, such as point *T*, which indicates the target position. The machine reference frame with coordinate $x_0y_0z_0$ is placed at point *O*, the centroid of the top surface of machine base. It is assumed in this kinematic analysis that the machine is at a position when *A* and *B* are at the coordinate positions $(0, h_1, d_1)$ and $(d_2, h_2, 0)$, respectively; here h_1, d_1, h_2, d_2 are the offset values of the origins of the coordinate systems for the *x* and *z* stages. The reference frame $x_ty_tz_t$ is placed at point *T*, where the direction of axis z_t indicates the orientation of the target, and (t_x, t_y, t_z) represents the coordinate position of the target *T* with respect to the reference coordinate $x_wy_wz_w$, placed at the centre of the target interface wheel *H*.

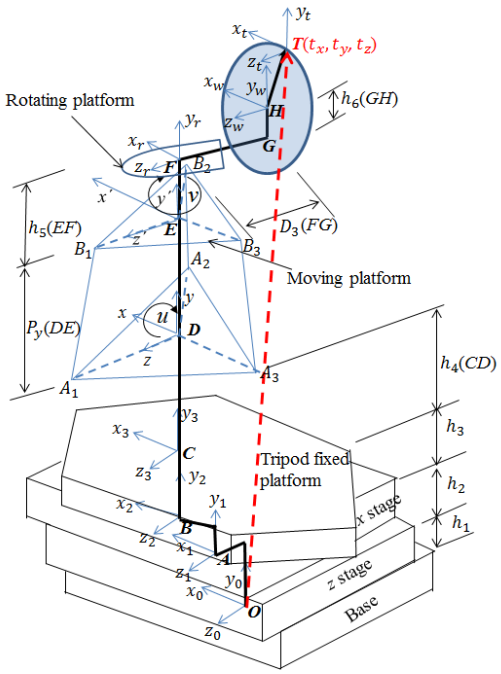

Figure 2. Kinematic model of HAMS.

As shown in Figure 2, the RPS parallel structure has three kinematic chains. In each chain, a variable length leg with actuated prismatic joint is connected to the fixed tripod platform by revolute joints (A_1, A_2 or A_3), and to the moving platform by spherical joints (B_1, B_2 or B_3). Both platforms $A_1A_2A_3$ and $B_1B_2B_3$ form equilateral triangle, and their centroids are at *D* and *E*, respectively. The Cartesian coordinate reference frame *xyz* for triangle $A_1A_2A_3$, is placed at *D*, while the reference frame *x'y'z'* for triangle $B_1B_2B_3$, is placed at *E* (where, $EB_1 = EB_2 = EB_3 = h$). Point *E* should ideally be directly above point *D* when HAMS is in its home position (zero position) and is

error free. Furthermore, point *F* is considered as the centroid of the rotating platform and as the centre of tilt rotation when HAMS is error-free. For simplicity, in this paper, the platforms that provide the tip and tilt motions will be known as the moving platform and the rotating platform, respectively (Figure 2).

For the convenience of analysis, it is assumed that the *z* axis of the *xyz* coordinate system is aligned with vector $\overrightarrow{DA_1}$, with the *x* axis in the same plane of the fixed triangular platform $A_1A_2A_3$, while the *y* axis is normal to this plane and is pointing upward. It should be noted that, for the alignment of target *T*, $\overrightarrow{EF}$ should be parallel to $\overrightarrow{GH}$, which means that the orientation of the target wheel is only controlled by the moving platform, and by the rotating platform mounted on the moving platform.

3.2 Modelling technique

The kinematic analysis of HAMS employs the concept of the homogeneous transformation matrix (HTM), which is briefly discussed below. A 4 × 4 matrix is needed to represent the relative position and orientation of a rigid body in three dimensional space with respect to a given coordinate system [23,24]. For example,

$$T_n^R = \begin{bmatrix} O_{ix} & O_{iy} & O_{iz} & P_x \\ O_{jx} & O_{jy} & O_{jz} & P_y \\ O_{kx} & O_{ky} & O_{kz} & P_z \\ 0 & 0 & 0 & P_s \end{bmatrix} \quad (1)$$

where T_n^R is a HTM that represents the coordinate transformation to the reference coordinate frame $x_Ry_Rz_R$ from that of the rigid body frame $x_ny_nz_n$. Based on the definition of a HTM, if the position and orientation of the end-effector frame $x_ty_tz_t$ at *T*, with respect to the inertial reference frame $x_0y_0z_0$ at *O*, is represented by the HTM A_T, then the elements of A_T will depend on the three position and nine orientation parameters of frame $x_ty_tz_t$ with respect to the reference frame $x_0y_0z_0$. The matrix A_T is formed by multiplying the A_i matrices, where A_i represent the interconnected coordinates (say, *N* in total) between the points *O* and *T* [17]:

$$\boldsymbol{A_T = A_1A_2A_3 \ldots A_N}. \quad (2)$$

Equation (2), known as the "loop closure equation", provides six scalar equations which give the end effector coordinates x_T^{ideal}(no error) when the mechanism's structural parameter $\boldsymbol{s}$ (for example, offsets between the two links), and configuration parameter $\boldsymbol{c}$ (for example, joint angle) are known, as shown in the following equation [25]:

$$\boldsymbol{x_T^{ideal} = f^{ideal}(s, c)}. \quad (3)$$

However, when the errors are considered in the model, the loop closure equation becomes $\boldsymbol{A_{T_{err}}}$:

$$\boldsymbol{A_{T_{err}}} = \boldsymbol{A_1 E_1 A_2 E_2 A_3 E_3 \ldots A_N E_N} \quad (4)$$

where $\boldsymbol{E_i}$ represents the HTMs defining the errors related to the relevant coordinates between the points *O* and *T* [22].

The end-effector's coordinates can be calculated from equation (5) below, where $\boldsymbol{e}$ denotes the vector of the errors, connecting the ideal position of *T* to its real positon:

$$\boldsymbol{x_T^{real}} = \boldsymbol{f^{real}}(\boldsymbol{s}, \boldsymbol{c}, \boldsymbol{e}). \quad (5)$$

Thus, the end effector's position and orientation error $\Delta\boldsymbol{x}$ can be defined as the 6×1 matrix which represents the difference between the real position and orientation of the end-effector and the ideal one [24]:

$$\Delta\boldsymbol{x} = \boldsymbol{x_T^{real}} - \boldsymbol{x_T^{ideal}}. \quad (6)$$

Then, for a given set of errors, $\Delta\boldsymbol{x}$ can be calculated.

Considering that the modelling technique using loop closure equations outlines a general framework for the error analysis of a kinematic mechanism, it is worth paying attention to the following points for the case of an error analysis for a hybrid mechanism:

- $\boldsymbol{E_i}$, as represented in equation (4), defines the errors for a particular frame A_i. This definition is based on the fact that physical errors, examples given above, change the geometric properties of a mechanism, which may cause a particular frame A_i to be displaced (translationally and/or rotationally) from its ideal location to its real location. The position and orientation of the real frame $\boldsymbol{A_{i_{err}}}$ with respect to the ideal frame A_i can be represented by a 4×4 matrix $\boldsymbol{E_i}$. The rotation part of $\boldsymbol{E_i}$ (the first three columns of the matrix as per the definition of HTM in equation (1)) shows the orientation change of frame A_i due to rotational errors of the frame itself, while the translational part of $\boldsymbol{E_i}$ (the last column of the matrix as per the definition of HTM in equation (1)) shows the positional deviations of the frame A_i due to translational errors of the frame. In this way, the error components of $\boldsymbol{E_i}$ can be used to define the errors of a particular frame A_i.
- In many cases, the arrangements of the constraints, such as joints and bearings in a kinematic mechanism, can be conveniently replaced with an equivalent kinematic system. Consider a simple example of the arrangement of the constraints applied to a cube, as given by Hale (1999) [26]. Five constraints, as shown

in Figure 3, are applied to the cube in such an arrangement that all the constraint lines intersect at the axis located at the centre of the cube. Since there exists no constraint that can affect the moment about this axis because the lever arm length is zero, the cube is free to rotate about this axis. Thus, the arrangement of these five constraints can be uniquely defined by the body's single degree of freedom. As such, if a reference frame is placed at the centre of the cube, any physical changes in the arrangement of the five constraints will affect the position and orientation of the reference frame at the centre of the cube. Thus, for the purpose of the kinematic analysis of the cube, it is logical to consider that the study of the geometric properties of the centre of the cube will be equivalent to the study of the overall geometric properties of the cube. Therefore, an error definition matrix can be constructed for the frame of the centre of the cube, and the elements of the matrix will represent the rotational and/or translational errors of the overall kinematic arrangement of the cube. These errors will be known as the "generalised errors", while the equivalent point of the kinematic system (the centre of the cube of the above example) as a "reaction point" in this analysis.

- The kinematic links in a parallel mechanism work simultaneously to effect any change in the position and orientation of the moving platform. With careful study of the joints (constraints) in a parallel mechanism, it may be possible to establish reaction point/s and, hence, the use of generalised errors for the moving platform, instead of the use of the geometric errors of the individual joints associated with the moving platform. This could potentially simplify the kinematic analysis of a complex mechanism, such as a parallel or a hybrid mechanism, and could be effective in considering the error averaging effects of a parallel mechanism.

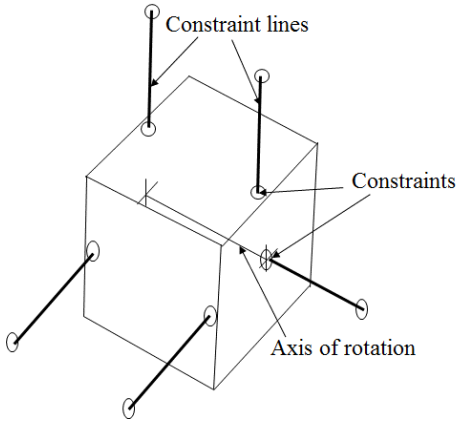

Figure 3. Five constraints applied to a cube result in a rotational degree of freedom at its centre [26].

3.3 Modelling the mechanism with no errors

As outlined in section 3.2, the first step to develop an error model to find the positional deviations at the target *T*, arising from the errors of the tip and tilt motions of HAMS, is to derive the expressions (see equation (3)) that describe the position of the target with respect to the reference coordinate when HAMS has error-free tip and tilt motions. Assuming the axes of the coordinate frames between *O* and *T* are initially parallel to the axes of the reference coordinate frame $x_0y_0z_0$, the desired orientation of *T*, as determined by the direction of the axis z_t, is achieved by Roll-Pitch-Yaw angles [23,27]. Using this representation, and following CLF's standard method of laser alignment, the desired orientation of the target *T* is achieved by three successive rotations of the frame $x_ty_tz_t$ about its coordinate axes: rotation α about the x_T axis or pitch, followed by rotation $\emptyset$ about the z_T axis or roll ($\emptyset = 0$ as per CLF's method), followed by a rotation β about y_T or yaw. This orientation can be achieved by the following transformation process of the frames as per equations (1) and (2), where $T_T^O(ideal)$ represents the ideal location (position and orientation) of the target with respect to the reference coordinate:

$$T_T^O(ideal)=T_{position}T_1T_2, \tag{7}$$

by using,

$$T_{position}=\begin{bmatrix}1&0&0& x+d_1+t_x\\0&1&0& P_y+h_1+h_2+h_3+h_4+h_5+h_6+t_y\\0&0&1& z+d_2+d_3+t_z\\0&0&0& 1\end{bmatrix} \tag{8}$$

where, x, P_y and z are the translational motions along the *x*, *y* and *z* axes of the reference frame $x_oy_oz_o$; t_x, t_y and t_z represent the values of the position vector of *T* with respect to coordinate $x_wy_wz_w$ at *H*; and $h_1, h_2, h_3, h_4, h_5, h_6, d_1, d_2$ and d_3 represent the offsets of the structure as shown in Figure 2. Also, by using

$$T_1=\begin{bmatrix}1&0&0&0\\0&\cos\alpha&\sin\alpha&0\\0&-\sin\alpha&\cos\alpha&0\\0&0&0&1\end{bmatrix} \tag{9a}$$

and

$$T_2=\begin{bmatrix}\cos\beta&0&-\sin\beta&0\\0&1&0&0\\\sin\beta&0&\cos\beta&0\\0&0&0&1\end{bmatrix}, \tag{9b}$$

$T_T^O(ideal)$ of equation (7) will have the following form:

$$T_T^O(ideal)=\begin{bmatrix} \cos\beta & 0 & -\sin\beta & x+d_1+t_x \\ \sin\alpha\sin\beta & \cos\alpha & \cos\beta\sin\alpha & P_y+h_1+h_2+h_3+h_4+h_5+h_6+t_y \\ \cos\alpha\sin\beta & -\sin\alpha & \cos\alpha\cos\beta & z+d_2+d_3+t_z \\ 0 & 0 & 0 & 1 \end{bmatrix}. \quad (10)$$

Equation (7) (also equation (10)) represents the coordinate relationship between the frames $x_0y_0z_0$ and $x_ty_tz_t$. This is shown in Figure 2 by drawing a thick black line from reference point *O* to *T* (that is, vector $\overrightarrow{OT}$). The same position and orientation of *T* can also be achieved with a vector $\overrightarrow{ODEFGHT}$ that connects *O* and *T* when going through the structure of HAMS; this vector is shown as a thick red dotted line in Figure 2. This latter vector can be determined by structural and configuration parameters, as given in equation (3).

Now consider the case when the target *T* needs to be placed at a desired location with the position (x, P_y, z) and with the orientation defined by the rotational angles α and β. This position of target *T* can be achieved by two translational motions of *x* and *z* along the x_2 and z_1 directions, given by the linear *xz* system, and one translational motion of P_y along the vertical *y* axis of the *xyz* frame, given by the parallel RPS mechanism (Figure 2). The desired orientation of the α and β angles can be achieved by the tip *u* and tilt *v* motions. Tip is the rotational motion of the RPS mechanism about the *x* axis of the *xyz* frame to orientate the moving platform with respect to *xyz*, while tilt is the rotational motion by the motor about the *y´* axis of the *x´y´z´* frame to orientate the rotating platform with respect to the *x´y´z´* frame. The transformation matrix which describes the orientation of the target through the use of tip *u* and tilt *v* angles is given by:

$$T_T^O(u-v)_{no\ error}=T_D^O T_E^D T(u)\, T_F^E T(v) T_H^F T_T^H, \quad (11)$$

where,

$$T_D^O=\begin{bmatrix} 1 & 0 & 0 & d_1 \\ 0 & 1 & 0 & h_1+h_2+h_3+h_4 \\ 0 & 0 & 1 & d_2 \\ 0 & 0 & 0 & 1 \end{bmatrix}, \quad (12a)$$

and

$$T_E^D=\begin{bmatrix} 1 & 0 & 0 & 0 \\ 0 & 1 & 0 & P_y \\ 0 & 0 & 1 & 0 \\ 0 & 0 & 0 & 1 \end{bmatrix}. \quad (12b)$$

The HTM to represent tip motion is given by

$$T(u) = \begin{bmatrix} 1 & 0 & 0 & 0 \\ 0 & \cos u & \sin u & 0 \\ 0 & -\sin u & \cos u & 0 \\ 0 & 0 & 0 & 1 \end{bmatrix}, \tag{13}$$

and

The HTM to represent tilt motion is given by

$$T(v) = \begin{bmatrix} \cos v & 0 & -\sin v & 0 \\ 0 & 1 & 0 & 0 \\ \sin v & 0 & \cos v & 0 \\ 0 & 0 & 0 & 1 \end{bmatrix}, \tag{14}$$

$$T_F^E = \begin{bmatrix} 1 & 0 & 0 & 0 \\ 0 & 1 & 0 & h_5 \\ 0 & 0 & 1 & 0 \\ 0 & 0 & 0 & 1 \end{bmatrix}, \tag{15a}$$

$$T_H^F = \begin{bmatrix} 1 & 0 & 0 & 0 \\ 0 & 1 & 0 & h_6 \\ 0 & 0 & 1 & d_3 \\ 0 & 0 & 0 & 1 \end{bmatrix}, \tag{15b}$$

$$T_T^H = \begin{bmatrix} 1 & 0 & 0 & t_x \\ 0 & 1 & 0 & t_y \\ 0 & 0 & 1 & t_z \\ 0 & 0 & 0 & 1 \end{bmatrix}. \tag{15c}$$

Substituting the values from the equations (12) to (15) into equation (11) yields:

$$T_T^O(u-v)_{no\ error} = \begin{bmatrix} \cos v & 0 & -\sin v & A_1 \\ \sin u \sin v & \cos u & \cos v \sin u & A_2 \\ \cos u \sin v & -\sin u \cos u \cos v & & A_3 \\ 0 & 0 & 0 & 1 \end{bmatrix} \tag{16}$$

and

$$A_1 = x + d_1 - d_3 \sin v + t_x cos\ v - t_z \sin v, \tag{17a}$$

$$A_2 = P_y + h_1 + h_2 + h_3 + h_4 + (h_5 + h_6 + t_y)\cos u + (d_3 + t_z)\cos v \sin u + t_x \sin u \sin v, \tag{17b}$$

and

$$A_3 = z + d_2 - (h_5 + h_6 + t_y)\sin u + (d_3 + t_z)\cos u \cos v + t_x \cos u \sin v. \tag{17c}$$

Comparison of the equation (10) with equation (16) shows that, for the target position of (x, P_y, z) and the orientation angles of α and β (pitch and yaw angles), both the vectors $\overrightarrow{OT}$ and $\overrightarrow{ODEFGHT}$, as shown in Figure 2, can give the same orientation of the target; however, positional deviations take place at the target for the vector $\overrightarrow{ODEFGHT}$. These deviations are due to the architectural structure of HAMS and are discussed in detail in section 4.

Subtracting equation (16) from equation (10) will give the positional deviations at the target *T* when HAMS has error-free tip and tilt motions:

$$D_{xt_{no\ error}} = t_x(\cos v - 1) - d_3 \sin v - t_z \sin v, \quad (18)$$

$$D_{yt_{no\ error}} = h_5(\cos u - 1) + h_6(\cos u - 1) + t_y(\cos v - 1) + (d_3 + t_z)\cos v \sin u + t_x \sin u \sin v, \quad (19)$$

$$D_{zt_{no\ error}} = d_3(\cos u \cos v - 1) + t_z(\cos u \cos v - 1) - (t_y + h_5 + h_6)\sin u + t_x \cos u \sin v. \quad (20)$$

3.4 Modelling for the mechanism with errors

It is clear that when geometric errors are present in the mechanism, the transformation matrix $T_T^O(u-v)_{no\ error}$ (equation (16)) will not be the same, since the spatial relationships among the frames between the points *O* and *T* will change (Figure 2). These geometric errors generally arise from the manufacturing and assembly errors of the components of the RPS mechanism and of the rotating platform actuated by the motor.

3.4.1 Error definitions

Assuming that parallelism and vertical errors of the HAMS are generally negligible, errors associated with the tip and tilt motions are considered in this kinematic model since they affect both the position and orientation of the target during its alignment. Tip and tilt errors are modelled as the "generalised errors" for this hybrid mechanism.

The tip error is related to the RPS mechanism. The RPS mechanism is a spatial mechanism which can provide three DOFs, that is rotational motions about the *x* and *z* axes (HAMS does not utilise rotation about the *z* axis and, hence, this rotation is ignored in this model) and translational motion along the *y* axis (all motions are with respect to the *xyz* frame of the RPS mechanism, as shown in Figure 2 and Figure 4, left), restricting the three other motions, that is translations along the *x* and *z* axes, and rotation about the *y* axis. However, the tip motion *u* of this mechanism induces small amount of translation motions $\delta_{x_{err}}$ and $\delta_{z_{err}}$ at point *E* along the *x* and *z* directions (note that *E* is the centroid of the moving platform, and is the origin of the coordinate frame *x´y´z´* of the moving platform), and a rotation u_{err} about the vertical direction *y* (Figure 4, left). Since these parasitic motions take place in the

constrained directions of the motion for the RPS mechanism, they may have an unwanted "decentering" effect on the moving platform, resulting in the positional deviations at the target T [22,28].

A typical HTM to represent these parasitic errors of HAMS can be written as:

$$T(u)_{error}=(T(u)_{err})_{pos.dev.}T(u)\ T(u_{err}) \tag{21}$$

where,

$T(u)$= HTM for tip motion, given in equation (13),

The HTM to represent the positional deviations at E is given by

$$(T(u)_{err})_{pos.dev.} = \begin{bmatrix} 1 & 0 & 0 & \delta_{x_{err}} \\ 0 & 1 & 0 & 0 \\ 0 & 0 & 1 & \delta_{z_{err}} \\ 0 & 0 & 0 & 1 \end{bmatrix}, \tag{22}$$

The HTM to represent the rotational error u_{err} about y is given by

$$T(u_{err})= \begin{bmatrix} \cos u_{err} & 0 & -\sin u_{err} & 0 \\ 0 & 1 & 0 & 0 \\ \sin u_{err} & 0 & \cos u_{err} & 0 \\ 0 & 0 & 0 & 1 \end{bmatrix}. \tag{23}$$

Substituting the values from the equations (22) and (23) and the value of $T(u)$ into equation (21) provides:

$$T(u)_{error}= \begin{bmatrix} \cos u_{err} & 0 & -\sin u_{err} & \delta_{x_{err}} \\ \sin u \sin u_{err} & \cos u & \cos u_{err} \sin u & 0 \\ \cos u \sin u_{err} & -\sin u & \cos u \cos u_{err} & \delta_{z_{err}} \\ 0 & 0 & 0 & 1 \end{bmatrix}. \tag{24}$$

The translational motion errors $\delta_{x_{err}}$ and $\delta_{z_{err}}$, and the rotational motion error u_{err} can be determined using the experimental or the analytical technique as discussed in sections 3.5.1 and 4.

It is important to note that the HTM for $(u)_{error}$ in equation (21) is written for the point E, the centroid of the moving platform as shown in Figure 2 and Figure 4, left. As will be seen in section 3.5, centroid E plays an important role in writing the constraint equations of the moving platform of the RPS mechanism. This is because the planes in which the spherical joints (B_1, B_2 and B_3 of Figure 2) of the moving platform are allowed to move in the error-free tip motion must intersect at point E [27,28]. Geometric errors associated with B_1, B_2 and B_3 will affect the position and orientation of point E. Therefore, E can be considered as the reaction point of the moving platform of the RPS mechanism, and the errors related to the point E, as shown in $T(u)_{error}$, are called the generalised error parameters in this analysis.

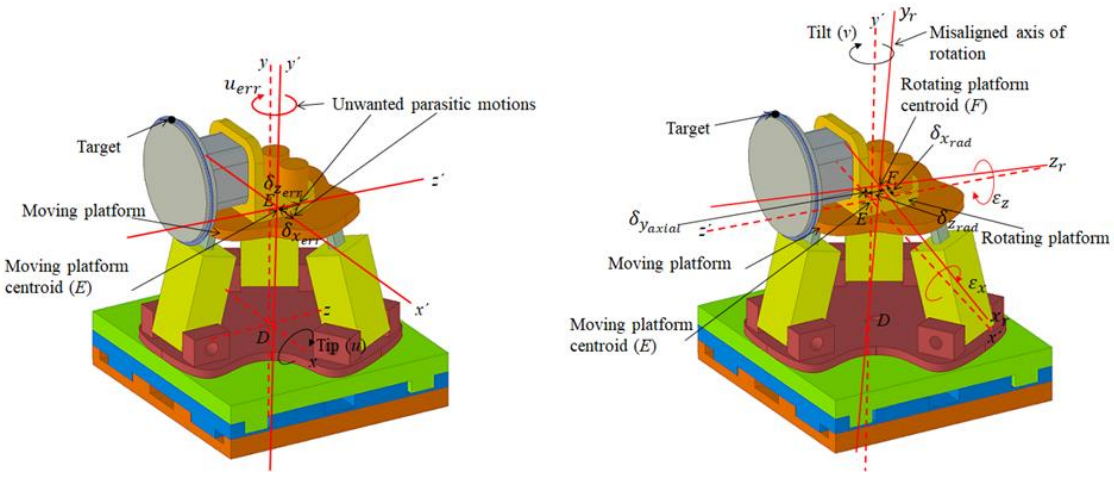

Figure 4. Rotational error motions of HAMS: for tip (left) and tilt (right).

The tilt errors are generated from the tilt motion of HAMS, which is the rotation of the rotating platform about the axis *EF*, as shown in Figure 2, to orientate the platform with respect to the moving platform's reference frame $x'y'z'$. Ideally, a rotating body should rotate about its axis of rotation without any error (*EF* should be aligned); however, in reality the axis of rotation of the rotating stage y_r revolves around y' with two radial errors $\delta_{x_{rad}}$ and $\delta_{z_{rad}}$ along the x' and z' axes, one axial error $\delta_{y_{axial}}$ along the y'axis and two tilt errors ε_x and ε_z about the x' and z' axes (Figure 4, right) [24]. Note that these six error parameters are enough to describe the positional and orientation changes of the centre of rotation *F*. Therefore, *F* can be considered as the reaction point for the rotating platform, while the six error parameters as the generalised error parameters for the tilt motion. These error motions can be described by the following HTM

$$T(v)_{error}=(T(v)_{err})_{pos.dev.}T(v)\ T(\varepsilon_x)\ T(\varepsilon_z) \tag{25}$$

where,

$T(v)$=HTM for tilt motion, given in equation (14),

The HTM to represent the positional deviations at *F* is given by

$$(T(v)_{err})_{pos.dev.}=\begin{bmatrix}1&0&0&\delta_{x_{rad}}\\0&1&0&\delta_{y_{axial}}\\0&0&1&\delta_{z_{rad}}\\0&0&0&1\end{bmatrix}, \tag{26}$$

The HTM to represent the rotational error ε_x about x' is given by

$$T(\varepsilon_x)=\begin{bmatrix}1 & 0 & 0 & 0\\ 0 & \cos\varepsilon_x & \sin\varepsilon_x & 0\\ 0 & -\sin\varepsilon_x & \cos\varepsilon_x & 0\\ 0 & 0 & 0 & 1\end{bmatrix}, \tag{27}$$

The HTM to represent rotational error ε_z about z' is given by

$$T(\varepsilon_z)=\begin{bmatrix}\cos\varepsilon_z & -\sin\varepsilon_z & 0 & 0\\ \sin\varepsilon_z & \cos\varepsilon_z & 0 & 0\\ 0 & 0 & 1 & 0\\ 0 & 0 & 0 & 1\end{bmatrix}. \tag{28}$$

After substituting the values from the equations (26) to (28) and the value of $T(v)$ into equation (25) yields (a first order approximation is applied for the expression $T(v)\,T(\varepsilon_x)\,T(\varepsilon_z)$, since the error terms are considered small compared to the tip and tilt motions):

$$T(v)_{error}=T_{tilt\,err}=\begin{bmatrix}\cos v & A & -\sin v & \delta_{x_{rad}}\\ \varepsilon_z & 1 & \varepsilon_x & \delta_{y_{axial}}\\ \sin v & B & \cos v & \delta_{z_{rad}}\\ 0 & 0 & 0 & 1\end{bmatrix} \tag{29}$$

where,

$A = (\sin v\,\varepsilon_x - \cos v\ \varepsilon_z)$, (30a)

and

$B =(-\sin v\,\varepsilon_z - \cos v\ \varepsilon_x)$. (30b)

Generalised error parameters for tilt *v* (three translational motion errors and two rotational motion errors, that is $\delta_{x_{rad}}$, $\delta_{z_{rad}}$, $\delta_{y_{axial}}$, ε_x and ε_z) can be determined using the experimental or analytical technique, as will be described in sections 3.5.2 and 4.

3.4.2 Model analysis: tip error only

The transformation matrix, which describes the position and orientation of target *T* when tip errors are considered (no error from the tilt), can be described as follows:

$$T_T^O(u-v)_{tip\,error}=T_D^O T_E^D T(u)_{error}\,T_F^E T(v) T_H^F T_T^H \tag{31}$$

where T_D^o, T_E^D, T_F^E, $T(v)$, T_H^F, T_T^H are as before, and $T(u)_{error}$ is shown in equation (24).
Substituting above values into equation (31) yields:

$$T_T^O(u-v)_{tip\,error}=\begin{bmatrix}J_1 & 0 & J_4 & B_1\\ J_2 & \cos u & J_5 & B_2\\ J_3 & -\sin u & J_6 & B_3\\ 0 & 0 & 0 & 1\end{bmatrix} \tag{32}$$

where,

$$J_1 = \cos v \cos u_{err} - \sin v \sin u_{err}, \tag{33a}$$

$$J_2 = \cos v \sin u \sin u_{err} + \sin u \sin v \cos u_{err}, \tag{33b}$$

$$J_3 = \cos u \cos v \sin u_{err} + \cos u \sin v \cos u_{err}, \tag{33c}$$

$$J_4 = -\cos v \sin u_{err} - \sin v \cos u_{err}, \tag{34a}$$

$$J_5 = \cos v \sin u \cos u_{err} - \sin u \sin v \sin u_{err}, \tag{34b}$$

$$J_6 = \cos u \cos v \cos u_{err} - \cos u \sin v \sin u_{err}, \tag{34c}$$

$$B_1 = \delta_{x_{err}} + x + d_1 - d_3(\cos v \sin u_{err} + \sin v \cos u_{err}) + t_x(\cos v \cos u_{err} - \sin v \sin u_{err}) - t_z(\cos v \sin u_{err} + \sin v \cos u_{err}), \tag{35a}$$

$$B_2 = P_y + h_1 + h_2 + h_3 + h_4 + (h_5 + h_6 + t_y)\cos u + d_3 \sin u\,(\cos v \cos u_{err} - \sin v \sin u_{err}) + t_x \sin u\,(\cos v \sin u_{err} + \sin v \cos u_{err}) + t_z \sin u\,(\cos v \cos u_{err} - \sin v \sin u_{err}), \tag{35b}$$

$$B_3 = \delta_{z_{err}} + d_2 + z - (h_5 + h_6 + t_y)\sin u + d_3 \cos u\,(\cos v \cos u_{err} - \sin v \sin u_{err}) + t_x \cos u\,(\cos v \sin u_{err} + \sin v \cos u_{err}) + t_z \cos u\,(\cos v \cos u_{err} - \sin v \sin u_{err}). \tag{35c}$$

The positional deviations at the target *T* as a result of the combined effects of tip motion errors and the architecture of HAMS can be found by subtracting equation (32) from equation (10):

$$D_{xt_{tip\ error+arch.}} = \delta_{x_{err}} - (d_3 + t_z)(\cos v \sin u_{err} + \sin v \cos u_{err}) + t_x(\cos v \cos u_{err} - \sin v \sin u_{err} - 1), \tag{36}$$

$$D_{yt_{tip\ error+arch}} = (h_5 + h_6 + t_y)(\cos u - 1) + (d_3 + t_z)\sin u\,(\cos v \cos u_{err} - \sin v \sin u_{err}) + t_x \sin u\,(\cos v \sin u_{err} + \sin v \cos u_{err}), \tag{37}$$

$$D_{zt_{tip\ error+arch}} = \delta_{z_{err}} - (h_5 + h_6 + t_y)\sin u + (d_3 + t_z)(\cos u \cos v \cos u_{err} - \cos u \sin v \sin u_{err} - 1) + + t_x \cos u\,(\cos v \sin u_{err} + \sin v \cos u_{err}). \tag{38}$$

If the generalised error parameters for the tip motion $\delta_{x_{err}}$, $\delta_{z_{err}}$ and u_{err} of the RPS mechanism and the offset values of the hybrid mechanism, such as h_5, d_3 and t_x, are known, the positional deviations of the target in the x_0, y_0 and z_0 directions can be calculated from the equations (36) to (38) for particular *u* and *v* angles.

3.4.3 Model analysis: tilt error only

The transformation matrix that describes the position and orientation of the target *T* when tilt (*v*) errors are considered (no error from the tip motion) can be described as follows:

$$T_T^O(u-v)_{tilt\ error}=T_D^O T_E^D T(u)\ T_F^E T(v)_{error} T_H^F T_T^H \tag{39}$$

where $T_D^o, T_E^D, T_F^E, T(u), T_H^F, T_T^H$ are the same as before and $T(v)_{error}$ is shown in equation (29).
Substituting above values into equation (39) provides:

$$T_T^O(u-v)_{tilt\ error}=\begin{bmatrix} \cos v\ K_3 & -\sin v\ C_1 \\ K_1 \quad K_4 & K_6 \quad C_2 \\ K_2 \quad K_5 & K_7 \quad C_3 \\ 0 \quad 0 & 0 \quad 1 \end{bmatrix} \tag{40}$$

where,

$$K_1 = \cos u\ \varepsilon_z + \sin u \sin v, \tag{41a}$$

$$K_2 = \cos u \sin v - \sin u\ \varepsilon_z, \tag{41b}$$

$$K_3 = \sin v\ \varepsilon_x - \cos v\ \varepsilon_z, \tag{42a}$$

$$K_4 = \cos u - \sin u\ (\cos v\ \varepsilon_x + \sin v\ \varepsilon_z), \tag{42b}$$

$$K_5 = -\sin u - \cos u\ (\cos v\ \varepsilon_x + \sin v\ \varepsilon_z), \tag{42c}$$

$$K_6 = \sin u \cos v + \cos u\ \varepsilon_x, \tag{43a}$$

$$K_7 = \cos u \cos v - \sin u\ \varepsilon_x, \tag{43b}$$

$$C_1 = \delta_{x_{rad}} + x + d_1 - d_3 \sin v + t_x \cos v - t_z \sin v - h_6\ (\cos v\ \varepsilon_z - \sin v\ \varepsilon_x) - t_y\ (\cos v\ \varepsilon_z - \sin v\ \varepsilon_x), \tag{44a}$$

$$C_2 = P_y + h_1 + h_2 + h_3 + h_4 + \left(h_5 + \delta_{y_{axial}}\right)\cos u + \delta_{z_{rad}} \sin u + \cos u + (h_6 + t_y)(\cos u - \sin u\ (\cos v\ \varepsilon_x + \sin v\ \varepsilon_z)) + (d_3 + t_z)(\cos v \sin u + \cos u\ \varepsilon_x) + t_x(\cos u\ \varepsilon_z + \sin u \sin v), \tag{44b}$$

$$C_3 = \delta_{z_{rad}} \cos u - \delta_{y_{axial}} \sin u + d_2 + z - h_5 \sin u - (h_6 + t_y)(\sin u + \cos u\ (\cos v\ \varepsilon_x + \sin v\ \varepsilon_z)) + (d_3 + t_z)(\cos u \cos v - \sin u\ \varepsilon_x) + t_x(\cos u \sin v - \sin u\ \varepsilon_z) \tag{44c}$$

The positional deviations at the target *T* as a result of the combined effects of tilt motion errors and the architecture of HAMS can be found by subtracting equation (40) from equation (10):

$$D_{xt_{tilt\ error+arch.}} = \delta_{x_{rad}} - (d_3 + t_z)\ \sin v + t_x(\cos v - 1) - h_6\ (\cos v\ \varepsilon_z - \sin v\ \varepsilon_x) - t_y\ (\cos v\ \varepsilon_z - \sin v\ \varepsilon_x), \tag{45}$$

$$D_{yt_{tilt\,error+arch}} = \delta_{y_{axial}}\cos u + h_5(\cos u - 1) + \delta_{z_{rad}}\sin u + (h_6 + t_y)(\cos u - \sin u\,(\cos v\,\varepsilon_x + \sin v\,\varepsilon_z) - 1) + (d_3 + t_z)(\cos v \sin u + \cos u\,\varepsilon_x) + t_x(\cos u\,\varepsilon_z + \sin u \sin v),$$

(46)

$$D_{zt_{tilt\,error+arch}} = \delta_{z_{rad}}\cos u - \delta_{y_{axial}}\sin u - h_5 \sin u - (h_6 + t_y)(\sin u + \cos u\,(\cos v\,\varepsilon_x + \sin v\,\varepsilon_z)) - +(d_3 + t_z)\,(\cos u \cos v - \sin u\,\varepsilon_x - 1) + t_x(\cos u \sin v - \sin u\,\varepsilon_z).$$

(47)

For the known generalised error parameters of the tilt motion, $\delta_{x_{rad}}$, $\delta_{y_{axial}}$, $\delta_{z_{rad}}$, $\delta_{z_{err}}$, ε_x and ε_z, of the rotating stage, and for the known offset values of the hybrid mechanism, such as h_5, d_3 and t_x, the positional deviations at the target in the x_0, y_0 and z_0 directions can be calculated from the equations (45) to (47) for particular *u* and *v* angles.

3.5 Analytical equations to describe the relations between the error parameters

Equations (36) to (38) and (45) to (47) show that for a set of tip, tilt and structural parameters, positional deviations at the target *T* due to tip and tilt errors can be determined, given that generalised error parameters, such as $\delta_{x_{err}}$, $\delta_{z_{err}}$, u_{err}, $\delta_{x_{rad}}$, $\delta_{z_{rad}}$, ε_x and ε_z, of the mechanism are known. These generalised error parameters can be determined using the experimental techniques as discussed in section 4. In the following section, the relationships between the error parameters are examined analytically.

3.5.1 Tip error parameters

In the RPS mechanism, the presence of parasitic motions $\delta_{x_{err}}$, $\delta_{z_{err}}$ and u_{err} causes positional deviations at point *E* and a rotation around the vertical direction at point *E*. These undesirable parasitic motions (also called the constrained variables) are related to the unconstrained or given variables (three DOFs, which are the desirable motions) of the RPS mechanism by the constraint equations. The constraint equations describe the relationships between these two types of variables based on certain geometric constraint(s) of the mechanism. The derivation of the constraint equations of the RPS mechanism is given in Appendix 1, but the equations are discussed in the following with some detail [19,27].

Consider a RPS mechanism, as shown in Figure 5, the structure of which is briefly described in section 3.1. The position and orientation of the moving platform $B_1B_2B_3$ with respect to the fixed platform $A_1A_2A_3$ can be described by a position vector $\overrightarrow{DE}$ and by a 3×3 rotation matrix T_E^D as shown below:

$$T_E^D = \begin{bmatrix} n_x & p_x & l_x \\ n_y & p_y & l_y \\ n_z & p_z & l_z \end{bmatrix}, \tag{48}$$

where ***n***, ***p*** and ***l*** are the unit vectors along *n*, *p* and *l* axes of the moving platform,

and

$$\vec{P} = \begin{bmatrix} p_x \\ p_y \\ p_z \end{bmatrix}. \tag{49}$$

In the RPS mechanism, each leg is connected to the fixed base by a revolute joint (A_1, A_2 or A_3) and to the moving platform by a spherical joint (B_1, B_2 or B_3). Therefore, each leg's motion is constrained in one of the following three planes:

$$p_x + hl_x = 0, \tag{50}$$

$$p_x + \frac{\sqrt{3}h}{2}n_x - \frac{1}{2}hl_x = -\sqrt{3}(p_z + \frac{\sqrt{3}h}{2}n_z - \frac{1}{2}hl_z), \tag{51}$$

$$p_x - \frac{\sqrt{3}h}{2}n_x - \frac{1}{2}hl_x = \sqrt{3}(p_z - \frac{\sqrt{3}h}{2}n_z - \frac{1}{2}hl_z). \tag{52}$$

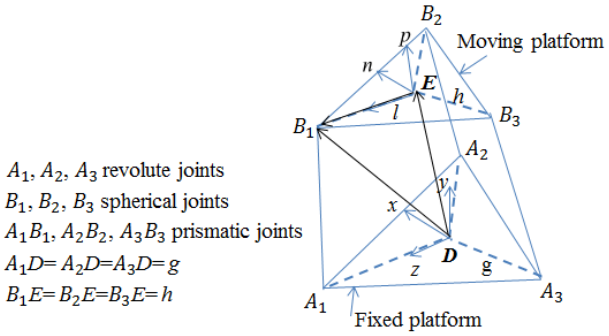

Figure 5. Spatial 3 DOF RPS parallel mechanism.

The following two equations can be obtained from equations (50) to (52):

$$l_x = n_z, \tag{53}$$

and

$$p_z = \frac{1}{2}h(l_z\text{-}n_x). \quad (54)$$

Equations (50), (53) and (54) are the constraint equations of the RPS mechanism. Equation (53) shows the constraint imposed on the orientation of the moving platform, while equations (50) and (54) relate the constraint variables p_x and p_z to the orientation of the moving platform as represented by n_x, l_x, n_z and l_z. For the error analysis of the RPS mechanism of HAMS, p_x and p_z of equations (50) and (54) can be replaced with the positional deviations of the centroid of the moving platform of the tripod, that is $\delta_{x_{err}}$ and $\delta_{z_{err}}$, where the n_x, l_x, n_z and l_z values can be determined from the moving platform's orientation, as shown in equation (24). Therefore, positional deviations at *E* due to parasitic motions of the RPS mechanism of HAMS can be determined by writing the constraint equations (50) and (54) for the HAMS' RPS mechanism, considering the generalised error parameters $\delta_{x_{err}}$, $\delta_{z_{err}}$ and u_{err} for the tip motion. The constraint equations that represent the positional deviations at *E* of the HAMS' RPS mechanism take the following form:

$$\delta_{x_{err}} = h \sin u_{err} \quad (55)$$

$$\delta_{z_{err}} = \frac{h \cos u_{err}(\cos u - 1)}{2}. \quad (56)$$

The error parameters $\delta_{x_{err}}$, $\delta_{z_{err}}$ and u_{err} can be measured experimentally; however, an alternative strategy to determine the rotational error motion of the RPS mechanism can be outlined as follows: the positional deviations of the centroid of the moving platform *E* in the *x* and *z* directions, when measured, represent $\delta_{x_{err}}$ and $\delta_{z_{err}}$ of the equations (55) and (56). Then, for the particular values of u and v angles, and for the known radius of the moving platform h (see Figure 5), the parasitic angular error motion u_{err} can be determined from the stated equations. However, the accuracy of determining u_{err} will depend on the ability of measuring the positional deviations at or very close to the centroid *E*. This may be difficult to achieve in some cases, for example, due to not being able to place the reflector of an interferometer at point *E*. In such cases, offsets in the *x* and *z* directions, arising from the placement of the measurement equipment, may need to be taken into considerations, and u_{err} should be determined using equations (36) and (38), along with the equations (55) and (56) (offset d_3 of equations (36) and (38) will be replaced with the offset that arise from the placement of the measurement equipment).

3.5.2 Tilt error parameters

Ideally, in the absence of the errors that may arise from the tilt motion, the centroids of the moving stage and the rotating stage, that is *E* and *F* respectively, should be collinear (Figure 2 and Figure 4, right). However, when the rotating stage has a misaligned axis of rotation, then the centroid *F* will be positionally deviated from *E* in the *x′*, *y′* and *z′* directions by $\delta_{x_{rad}}$, $\delta_{y_{axial}}$ and $\delta_{z_{rad}}$. Consider that the new location of *F* is *F'*.

$$\overrightarrow{EF} = \begin{bmatrix} 0 \\ h_5 \\ 0 \end{bmatrix} \tag{57}$$

where, h_5 is the distance between *E* and *F* along the *y′* direction as shown in Figure 2.

The orientation of *F* with respect to *E* will take the form of a 3×3 rotation matrix T_F^E as shown below,

$$T_F^E = \begin{bmatrix} n'_x & p'_x & l'_x \\ n'_y & p'_y & l'_y \\ n'_z & p'_z & l'_z \end{bmatrix}. \tag{58}$$

Then, $\overrightarrow{EF'}$ can be written as,

$$\overrightarrow{EF'} = \begin{bmatrix} \delta_{x_{rad}} + h_5 p'_x \\ \delta_{y_{axial}} + h_5 p'_y \\ \delta_{x_{rad}} + h_5 p'_z \end{bmatrix} \tag{59}$$

Since $\overrightarrow{EF}$ and $\overrightarrow{EF'}$ should be collinear, the following constraint equations can be written for the rotating platform, noting that matrix T_F^E actually represents the orientation components of the matrix $T(v)_{error}$ of equation (29):

$\delta_{x_{rad}} + h_5 p'_x = 0$

which gives,

$$\delta_{x_{rad}} = h_5 (\sin v\, \varepsilon_x - \cos v\, \varepsilon_z) \tag{60}$$

and,

$\delta_{x_{rad}} + h_5 p'_z = 0$

which gives,

$$\delta_{z_{rad}} = -h_5 (\sin v\, \varepsilon_z + \cos v\, \varepsilon_x) \tag{61}$$

Similar to the case of tip error parameter determination, an alternative strategy to find the tilt error parameters ε_x and ε_z can be described as follows: the displacements at or near the centre of rotation of the rotating platform

F (that is, the reaction point of the rotating platform) in the *x´* and *z´* directions are measured to use in the equations (60) and (61), giving the tilt error parameters ε_x and ε_z for particular values of u, v and h_5. However, offsets arising from the placement of the measurement equipment may need to be dealt with the similar way as described in section 3.5.1 using equations (45) and (47) along with the above two equations.

4. Experimental validation of the error model

4.1 Experimental setup

The positional deviations in the *z* and *x* directions as a result of the error motions of tip and tilt were measured using an interferometer (Renishaw model XL-80). These measurements of the positional deviations were achieved by determining the linear displacements of the moving part (moving stage, rotating stage and target wheel) during the rotational motions of HAMS (*u* and *v*). In the interferometer set up (Figure 6), the reflector was mounted on the moving part using appropriate fixtures while using the beam-splitter as the fixed optic. The rotational motions considered in this study to measure the linear displacement were in the range of $\pm 1.4°$, which represents the typical tip and tilt motion range of the target alignment method of the CLF.

The error measurements were carried out following two steps:

1. Rotations u_{err}, ε_x and ε_z and linear displacements $\delta_{x_{err}}$, $\delta_{z_{err}}$, $\delta_{x_{rad}}$, $\delta_{z_{rad}}$ and $\delta_{y_{axial}}$ were measured for the moving stage and for the rotating stage by placing the reflectors as close to the centroid of the moving stage or the rotating stage as practicable (Figure 6*a*-*b*). The generalised error parameters thus measured actually represent the geometric errors originated from the RPS mechanism and from the motor, actuating the rotating platform.
2. Linear displacements were measured at the target (*T* as shown in Figure 1*a*) on the target interface wheel by placing the reflector as close to the target as feasible (Figure 6*c*). The displacements measured would represent the overall positional deviations of the target, arising from: (a) $\delta_{x_{err}}$, $\delta_{z_{err}}$, $\delta_{x_{rad}}$, $\delta_{z_{rad}}$, $\delta_{y_{axial}}$, as determined in the previous step and (b) the angular error components (u_{err}, ε_x and ε_z) that were magnified by the structural offsets of HAMS (see equations (36) to (38) and equations (45) to (47)).

Therefore, the error parameters, as determined in the step 1, were used in the displacement equations (equations (36) to (38) and (45) to (47)) of the error model to calculate the positional deviations of the target and the results were verified against experimentally-determined values, as described in step 2 of the measurements.

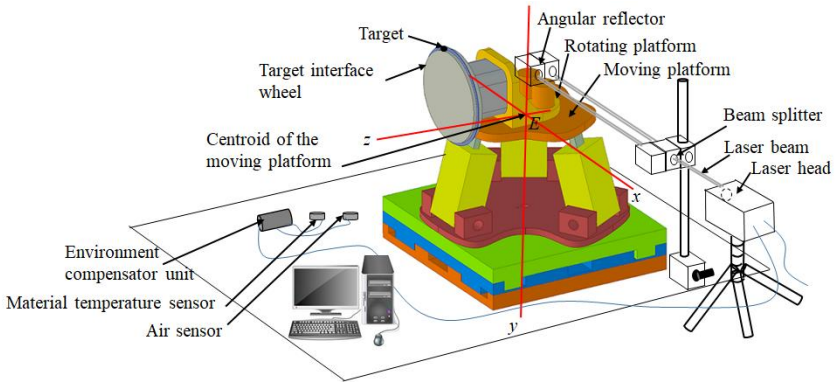

(a)

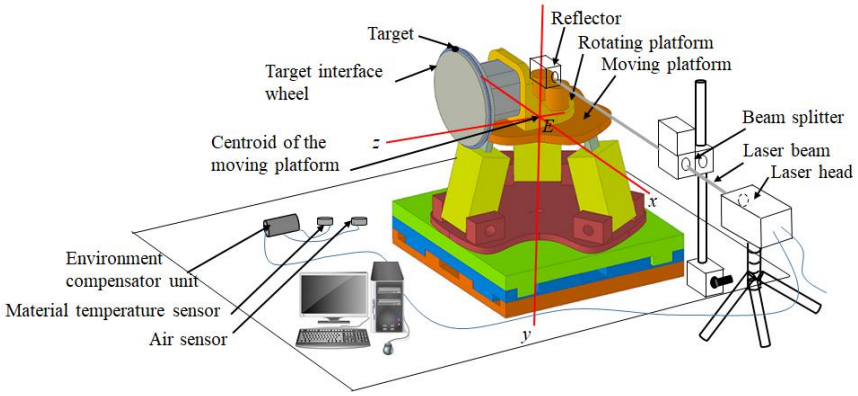

(b)

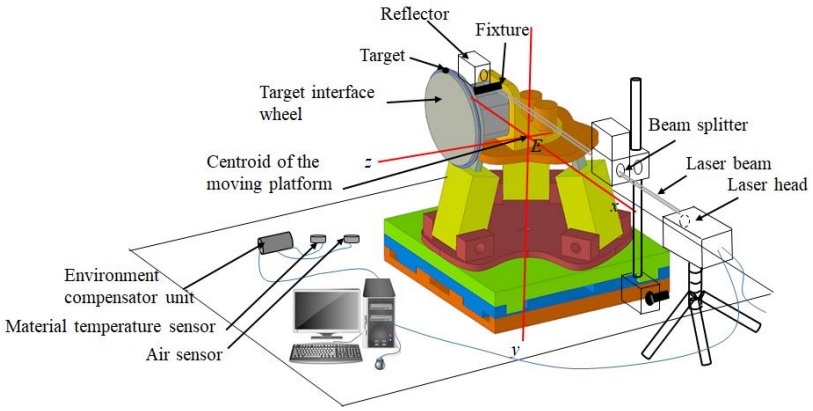

(c)

Figure 6. Schematic representation of the interferometer setup. The setups shown in the figure are to measure (a) the tip angular error u_{err} close to the centroid of the moving platform *E* (b) tip displacement error $\delta_{x_{err}}$ in the *x* direction close to *E*, and (c) positional deviation close to the target in the *x* direction $\delta_{x_{err}}$ due to tip motion.

Accuracies of the linear displacement measurements using interferometer are affected by the experimental errors that arise from the variations in air temperature, air pressure and relative humidity, since these environmental factors affect the reflective index of the ambient air [29,30]. Therefore, an environmental compensator unit (Renishaw model XC-80) was used to reduce these measurement errors. However, there will be other error sources that will contribute towards the measurement uncertainties, for example, (a) in the first step of the measurement stated above, the reflector should be ideally placed at the centroids of the moving stage and of the rotating stage. In reality, the reflector was placed slightly above the centroid due to inaccessibility to the centroid area; (b) the exact structural offsets of HAMS from the centroids were difficult to measure. However, with careful design of the setup of the experiment, it is possible to avoid some sources of experimental uncertainties and improve the measurement accuracy, for example, considering small tip angular motions, tip angular error u_{err} measurement (also tip displacement error $\delta_{x_{err}}$) carried out in the x direction (Figure 6*a*-*b*) will be more accurate than the measurement in the z direction. This is because the reflector's displacement in the x direction is negligibly affected by the tip rotation about x axis, and by the reflector's placement slightly above the centroid area. The overall measurement uncertainty arising from the repeatability of the measured distances and from the atmospheric effects was estimated not to exceed 200 nm (at a coverage factor $k = 2$, giving a confidence level of approximately 95%). The values of measurement uncertainty, compared to the positional deviations measured on the micrometre and millimetre scale, are not shown in the experimental results as they are negligibly small.

4.2 Results and discussion

The results shown here are the experimentally determined values of the positional deviations of the target *T* due to the tip and tilt motion errors, and they are compared with the positional deviations calculated by the equations derived in the error model. It is found that the predicted results from the error model agree well with the experimental results. The discrepancies between the two results can be attributed to the following: (a) the inaccuracy of the offset values of the hybrid mechanism that were measured and used in the calculations; (b) the inaccuracy of positioning the reflectors at the centroids of the stages or at the target; (c) model considered only the tip and tilt errors for the positional deviations of the target. In practice, there may be other minor sources of error, such as orthogonality and parallelism errors, that can affect the positional deviations of the target.

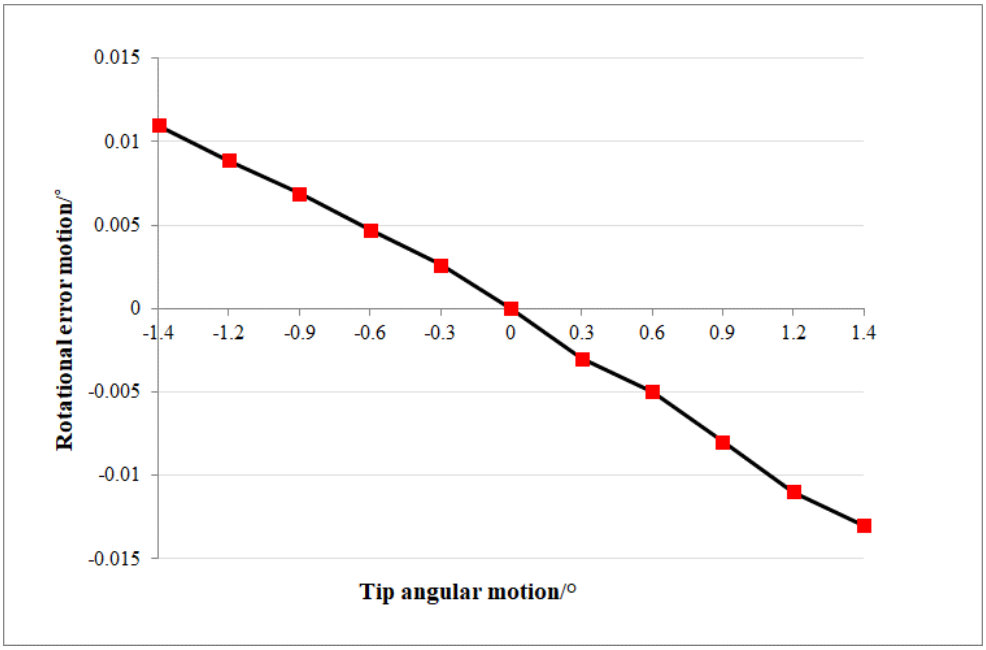

Figure 7. Rotational parasitic error motion of the RPS mechanism (tripod), representing a rotational motion about *y* axis of the reference frame *xyz*, as calculated from the model.

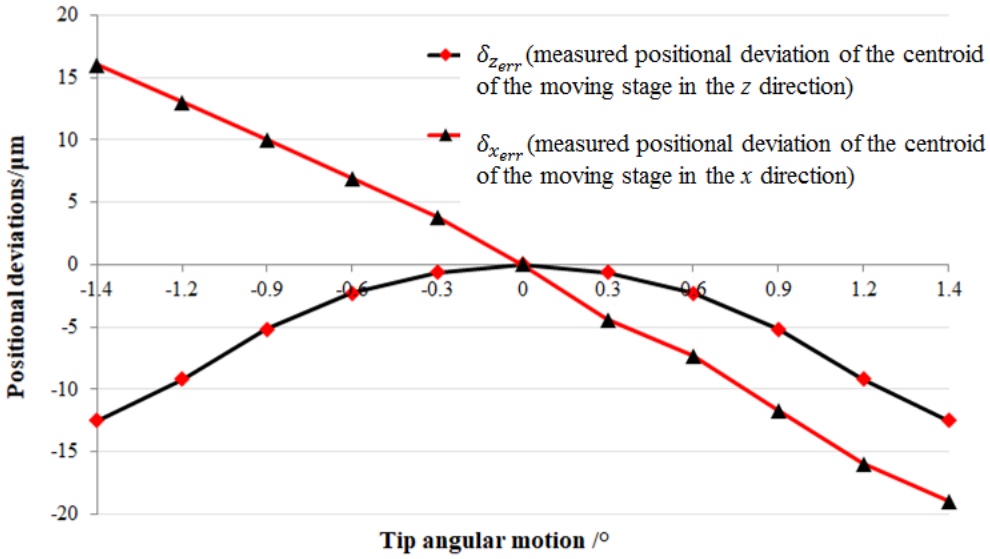

Figure 8. Linear displacements of the centroid of the moving platform along the *x* and *z* directions of the reference frame *xyz*; these displacements arise from the parasitic motions of RPS mechanism (tripod).

The important and interesting observations from the comparative study are as follows:

1. The rotational displacement and the linear displacements measured at the centroid position of the moving platform of the tripod represent the rotational parasitic error motion u_{err}, and two translational parasitic motions $\delta_{x_{err}}$ and $\delta_{z_{err}}$, respectively, of the RPS mechanism (Figure 7 and Figure 8). These translational parasitic motions, as explained in sections 3.4.1 and 3.5.1, represent two unwanted motions in the restricted directions, resulting in the positional deviations at the centroid of the moving platform in the *x* and *z* directions with respect to the reference frame *xyz* (see equation (24)), leading to the positional deviations at the target in the x_0 and z_0 directions of the reference frame $x_0y_0z_0$ (see equations (36) to (38)). However, of the three parasitic motions ($\delta_{x_{err}}$, $\delta_{z_{err}}$and u_{err} as shown in Figure 4, left), the rotational parasitic error motion u_{err} about *y* (this can also be determined using equations (55) and (56) as described in the sections 3.5.1) can have a significant effect on the positional deviations at the target. Figure 7 and Figure 8 show that tip causes very large positional deviations at the target, especially in the z_0 direction. One main source of these deviations is the Abbe offsets of HAMS, which amplify the rotational error u_{err}. In fact, the architecture of the upper part of the HAMS, which is mounted on the rotating platform, is such that the target on the target interface wheel is at offsets of 118 mm and 96 mm along the *y´* and *z´* directions, respectively, from the centroid *E* of the moving platform (Figure 9). If there were no offsets in the horizontal and vertical directions from this centroid, theoretically, there would only be the positional deviations at the target due to two parasitic translational motion errors $\delta_{x_{err}}$ and $\delta_{z_{err}}$ (see equations (55) and (56)).

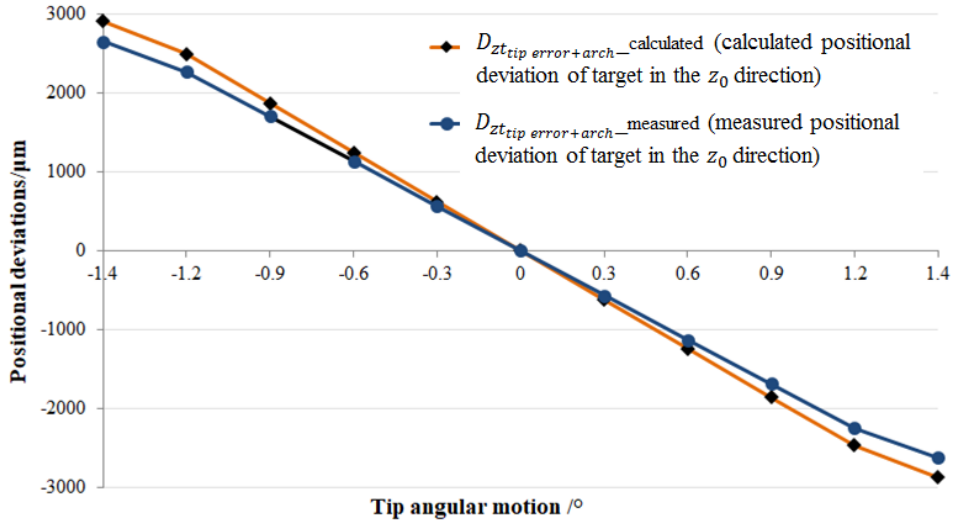

Figure 7. Comparison of the calculated and measured positional deviations of the target in the z_0 direction of the reference frame $x_0y_0z_0$ due to the tip motion and its associated parasitic errors.

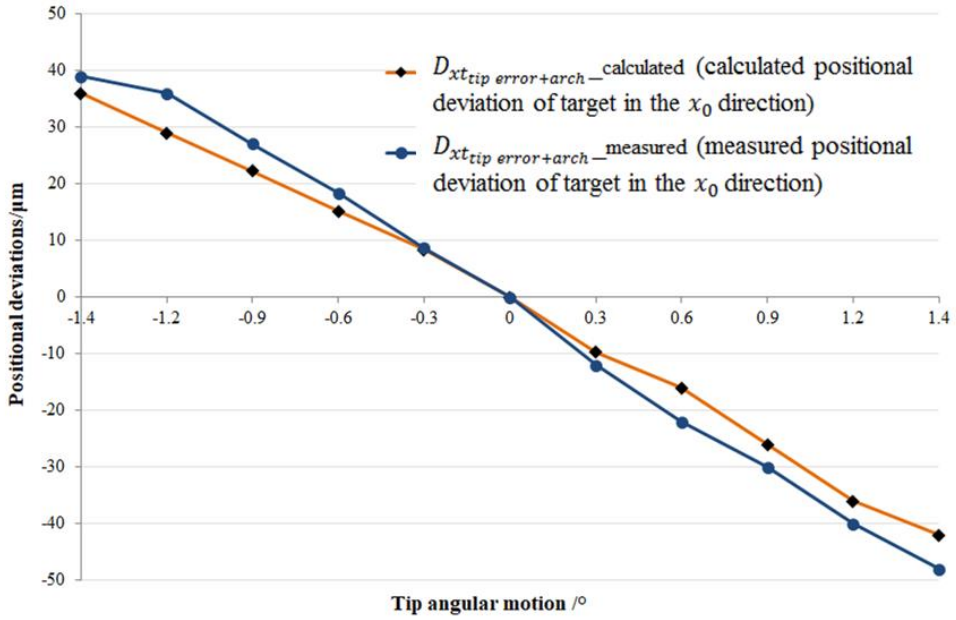

Figure 8. Comparison of the calculated and measured positional deviations of the target in the x_0 direction of the reference frame $x_0y_0z_0$ due to the tip motion and its associated parasitic errors.

2. It is not only this rotational error u_{err} that is amplified and causes the deviations at the target. The model predicts (from equations (18) to (20)) that the tip motion, even in the absence of all the parasitic motion errors, is responsible for considerable positional deviations at the target in the x_0 and z_0 directions, unless they are compensated by the HAMS' motion control software. These deviations are due to the Abbe offsets described before, and are shown in Figure 10. It is noteworthy in the figure that positional deviation at target in the x_0 direction is very small. Comparison of the Figure 10 with Figure 7 and 10 suggests that:
    - the main source of the positional deviation at the target in the z_0 direction is tip motion, as it is magnified by the 118 mm Abbe offset in the y' direction, as shown in Figure 9. Other displacements, namely translational parasitic motion $\delta_{z_{err}}$ and rotational parasitic motion u_{err}, when it is magnified by the 96 mm Abbe offset in the z' direction (see Figure 9), may have little effect on the positional deviation at the target in the z_0 direction;
    - the main source of the positional deviation at the target in the x_0 direction is mainly due to the parasitic angular error motion, u_{err}, as it is magnified by the 96 mm Abbe offset in the z' direction (see Figure 11). A small contribution towards this positional deviation may come from the

translational parasitic motion $\delta_{x_{err}}$. The effect of Abbe offset on the tip motion does not influence the positional deviation in the x_0 direction.

3. Following the above discussion, the measured positional deviations of the target due to the tip motion represent a cumulative sum of three types of displacement error:
    - positional deviations at the target due to the architecture (that is, structural offsets) of HAMS,
    - translational parasitic motions that are originated from the RPS mechanism,
    - positional deviations at the target caused by the magnification of the rotational parasitic motion of the RPS mechanism by the structural offsets.

    The equations derived in the model (equations (36) to (38)), therefore, have taken into considerations of all three types of error to calculate the positional deviations at the target.

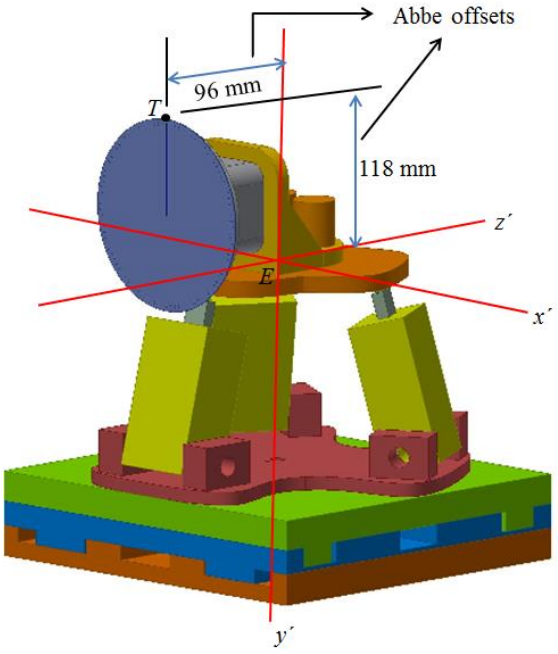

Figure 9. Abbe offsets of HAMS.

4. Similar to the case of the tip error motions, the positional deviations of the target due to the tilt motion and its associated error motions, as can be predicted from the model (equations (45) to (47)), include three types of displacement errors:
    - positional deviations at the target due to the architecture (that is, structural offsets) of HAMS,

- translational error motions of the rotating stage originated at the centroid of the rotating stage, due to the misaligned axis of rotation of the motor,
- positional deviations at the target caused by the magnification of the rotational errors, originated at the centroid of the rotating stage due to the misaligned axis of rotation of the motor, by the structural offsets.

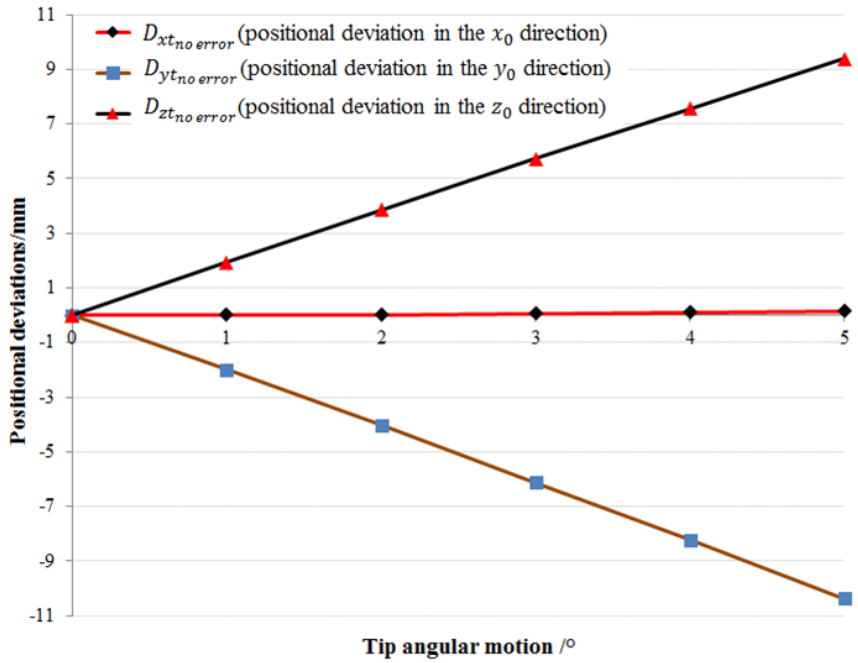

Figure 10. Theoretically calculated (equations (18) to (20)) positional deviations due to Abbe offsets at varying tip angular motions (no tilt motion or errors considered).

5. For the tilt motion, the experimental results and the model predictions suggest that tilt motion and its associated error motions ε_x, ε_z, $\delta_{x_{rad}}$ and $\delta_{z_{rad}}$, which originate at the centroid of the rotating platform due to the misaligned axis of rotation of motor (Figure 4, right), cause significant positional deviations at the target T in the x_0 and z_0 directions (Figure 11). The deviation in the x_0 direction is much higher compared to the deviation in the z_0 direction. Similar to the case of tip motion, this indicates that deviation in the x_0 direction is mainly due to the magnification of the tilt motion by the 96 mm Abbe offset along the z' direction (notice the second term in equation (45)). On the other hand, the positional deviation in the z_0 direction is mainly contributed by the errors ε_z and $\delta_{z_{rad}}$. In fact, ε_z is magnified by the 118 mm Abbe offset (along the y' direction), and the resultant distance in the x' direction (that is, sine error) is again liable to the magnification

by the tilt motion itself (note the fourth term of the equation (47)). It is also worth pointing out that, of the two rotational errors ε_x and ε_z, ε_z has more influence on the positional deviation at the target. This is because of the asymmetric architectural structure of the upper part of the HAMS, which is mounted on the rotating platform. It was observed that the target interface wheel situated in the overhanging structure was not accurately balanced by the masses placed in the opposite direction (along the z' direction) of the interface wheel (see Figure 1 and Figure 4). As such, the rotating platform was prone to rotate with an axis of rotation inclined towards the x' direction, making the error ε_z larger than ε_x.

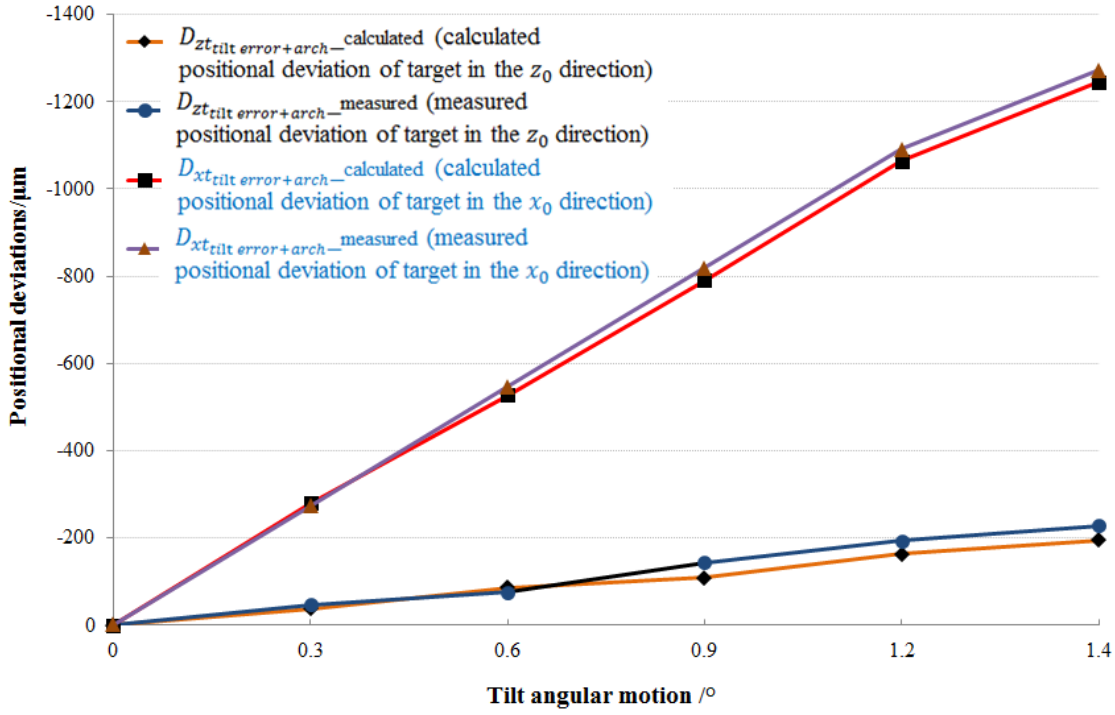

Figure 11. Comparison of the calculated and measured positional deviations of target (tool point) due to tilt rotational errors (in z_0 and x_0 directions).

6. The analyses stated above suggest that with its current performance level, CLF's hybrid mechanism HAMS is not capable of delivering the target to the laser focus with an accuracy of few micrometres. The performance improvement of HAMS will be covered elsewhere.

5. Conclusion

Developing a kinematic model is an important step to find the error compensation strategies for a hybrid kinematic mechanism, since the model helps quantifying the errors by deriving the analytical equations for the positional deviations at the target. In this paper, an error model is developed by establishing the kinematic relationships between the parallel mechanism and the other key components of the hybrid mechanism, and by considering the mechanism's two rotational motions (tip and tilt) and their associated error motions. Since, taking into account of the individual error sources of a complex mechanism, such as a hybrid or a parallel mechanism, can result in a complex error analysis, an alternative method to develop an error model is applied in this paper. This is done by establishing a small number of key points, called the reactions points, in the relevant kinematic systems of the mechanism, and by determining the reaction points' geometric errors that affect the rotational motions of the hybrid mechanism and, eventually, the ideal position of the target. A reaction point can be considered as an equivalent to a set of constraints that are present in a kinematic system of a mechanism. Essentially, the equivalent kinematic behaviour, such as degrees of freedom and geometric errors, of a reaction point should be able to sufficiently define the kinematic behaviour of the system it is representing. For example, in the error model, the centroid of the moving platform of the RPS mechanism is used as a reaction point for the moving platform, instead of considering all three spherical joints and three prismatic joints that connect the moving platform to the fixed platform. As such, three parasitic error motions related to the centroid of the moving platform are included in the model as tip error motions. It is found that the positional deviations at the target as determined by the equations of the model show good agreements with the experimentally determined positional deviations at the target. The errors associated with the reaction points are called the "generalised error" parameters in this paper, since these errors are enough to describe the deviations of the geometric properties of a set of constraints in a kinematic system. It is also found that of the two types of generalised error parameter for tip motion, rotational error parameter, as compared to translational parameters, have a significant influence on the final position of the target when the mechanism has considerable lateral offsets (measured from the reaction point to the target). For tilt motion, the centroid of the rotating platform is considered as the reaction point, and the errors that arise due to misaligned centre of rotation of the motor are considered as the generalised error parameters.

This paper demonstrates that generalised error parameters can be determined using analytical equations of the model and using experimental technique, which is, in this case, measuring the linear displacements with an interferometer. The parameters determined can be used to calculate the positional deviations at the target, which can be experimentally validated using the interferometer. The future work will focus on developing suitable error compensation strategies for HAMS based on the error model.

Acknowledgements

The authors gratefully acknowledge the help and support of Mr Sam Astbury and Mr Chris Spindloe of CLF (STFC) and Dr Wahyudin Syam and Mr Teguh Santoso of the University of Nottingham. The authors would especially like to thank Prof. Alex Slocum of Massachusetts Institute of Technology for his valuable comments. This research project is jointly funded by STFC (Oxfordshire, UK) and EPSRC (grants EP/M008993/1 and EP/L016567/1).

REFERENCES

[1] McKenna P, Quinn MN. Energetic electron generation and transport in intense laser-solid interactions. In: Mckenna P, Neely D, Bingham R, Jaroszynski DA, (ed.). Laser-plasma interactions and applications. Switzerland: Springer; 2013.

[2] Danson C, Hillier D, Hopps N. Petawatt class lasers worldwide. In: Lin Z, Danson C, (ed.). High power laser science and engineering. Shanghai: Chinese laser press Cambridge University Press; 2015.

[3] Spindloe C, Tolley MK, Hiscock P, Beardsley M, Spencer JJ. An update of target fabrication techniques for the mass production of advanced fast ignition cone targets. Fusion Sc. Technol. 2011;59(1):221-226

[4] Booth N, Clarke R, Heathcote R, Neely D, Pattathil R, Rusby D, Spindloe C, Symes D, Tolley MK. Tomlinson S. High-rep rate target development for ultra-intense interaction science at the central laser facility. Proc SPIE 2014;9211:1-8.

[5] Tolley M, Spindloe C. Microtargetry for high power lasers in laser-plasma interactions. In: Mckenna P, Neely D, Bingham R, Jaroszynski DA, (ed.). Laser-plasma interactions and applications. Switzerland: Springer; 2013.

[6] Symes DR, Booth N, Baraclough M, Indorf G, Oliver P, Scott GG, Neely D, Spindloe C, Heathcote RI, Clarke RJP, Foster S, Gregory CD, Rajeev PP. Progress on positioning of solid targets for Gemini. Central Laser Facility Annual Report 2014;15.

[7] Spindloe C, Arthur G, Hall F, Tomlinson S, Potter R, Kar S, Green J, Higgingbotham A, Booth N, Tolley M K. High volume fabrication of laser targets using MEMS techniques. J. Phys. Conf. Ser. 2016;713:012002.

[8] Booth N, Ettlinger O, Neely D, Pattathil R, Sellers A, Symes D. Target positioning and alignment of the Astra-Gemini facility. Proc SPIE 2013;8850:1-8.

[9] Niku SB. Introduction to robotics: analysis, control, applications. USA: Willey; 2011.

[10] Karim S, Weber U. Kinematic design. In: Leach RK, Smith ST, (ed.). Basics of precision engineering. New York: CRC Press; 2018.

[11] Allen JM, Axinte DA, Pringle T. Theoretical analysis of a special purpose miniature machine tool with parallel kinematic architecture: free leg hexapod. Proc. IMechE Part B: J. Eng. Manufac. 2011;226(3):412-430.

[12] Liu XJ, Wang J. Parallel kinematics: type, kinematics and optimal design. New York: Springer; 2014.

[13] Milutinovic M, Slavkovic N, Milutinovic D. Kinematic modelling of hybrid parallel serial five axis machine tool. FME Trans. 2013;41:1-10.
[14] Harib KH, Sharifullah AMM, Moustafa KAF. Optimal design for improved hybrid kinematic machine tools. Ann. CIRP 2013;12:109-14.
[15] Hu PH, Yu CW, Fan KC, Dang XM, Li RJ. Error averaging effect in parallel mechanism coordinate measuring machine. Appl. Sci. 2016;6:383-395.
[16] Wang FS, Chen SL. Geometric error measurement and compensation of a six-degree-of-freedom hybrid positioning stage. Proc. IMechE Part B: J. Eng. Man. 2008;222:185-200.
[17] Karim S, Piano S, Leach R, Tolley M. Error analysis for a high-precision five degree of freedom hybrid mechanism for high-power high-repetition rate laser system. In: Proc ASPE 32nd Annual Meeting 2017. p. 366-372.
[18] Ramesh R, Mannan M, Poo AN. Error compensation in machine tools - a review. Int. J. Mach. Tool. Manufac. 2000;40:1257-1284.
[19] Sartori S, Zhang GX. Geometric error measurement and compensation of machines. Ann. CIRP 1995;44: 599–609.
[20] Schwenke H, Knapp W, Haitjema H, Weckenmann A, Schmitt R, Delbressine F. Geometric error measurement and compensation of machines—an update. Ann. CIRP 2008;57(2):660-675.
[21] Chen SL, Chang TH, Hsei MH. Analytical modelling of the effects of manufacturing errors on the accuracy for a TRR-XY hybrid parallel link machine tool. Proc. Mech. Eng. 2001;215:1203-1216.
[22] Carretero JA, Phdhorodeski RP, Nahon MA, Gosselin CM. Kinematic analysis and optimisation of a new three degree of freedom spatial parallel manipulator. J. Mech. Design 2000;122:17-24.
[23] Seugling R. System modelling. In: Leach RK, Smith ST, (ed.). Basics of precision engineering. New York: CRC Press; 2018.
[24] Slocum AH. Precision machine design. New Jersey: Prentice-Hall; 1992.
[25] Mavroidis C, Dubowsky S. Drouet P, Hntersteiner J, Flax J. A Systematic error analysis of robotic manipulators: application to a high performance medical robot. Proc. IEEE 1997;980-985.
[26] Hale LC. Principles and techniques for designing precision machines. In: PhD thesis. Massachusetts Institute of Technology; 1999.
[27] Tsai LW. Robot Analysis: The mechanics of serial and parallel manipulators. USA: John Willey and Sons; 1999.
[28] Li Q, Herve JM. 1T2R Parallel mechanisms without parasitic motion. Proc. IEEE. 2010;26:401-410.
[29] Haitjema H. Achieving traceability and sub-nanometer uncertainty using interferometric techniques. Meas. Sci. Technol. 2008;19(8):1-6.
[30] Bonsch G, Potulski E. Measurement of the refractive index of air and comparison with modified Edlen's formulae. Metrologica 1998;35:133-139.

Appendix 1

As shown in Figure 5, $A_1A_2A_3$ and $B_1B_2B_3$ are equilateral triangles; therefore, the following equations can be written:

$$\overrightarrow{DA_1}=\begin{bmatrix}0\\0\\g\end{bmatrix} \qquad \overrightarrow{DA_2}=\begin{bmatrix}\frac{\sqrt{3}g}{2}\\0\\-\frac{1}{2}g\end{bmatrix} \qquad \overrightarrow{DA_3}=\begin{bmatrix}-\frac{\sqrt{3}g}{2}\\0\\-\frac{1}{2}g\end{bmatrix} \tag{62}$$

$$\overrightarrow{EB_1}=\begin{bmatrix}0\\0\\h\end{bmatrix} \qquad \overrightarrow{EB_2}=\begin{bmatrix}\frac{\sqrt{3}h}{2}\\0\\-\frac{1}{2}h\end{bmatrix} \qquad \overrightarrow{EB_3}=\begin{bmatrix}-\frac{\sqrt{3}h}{2}\\0\\-\frac{1}{2}h\end{bmatrix}. \tag{63}$$

The position vectors of B_1, B_2 and B_3 can be written as follows:

$$\overrightarrow{DB_1}=\begin{bmatrix}p_x+\ hl_x\\p_y+hl_y\\p_z+hl_z\end{bmatrix} \quad \overrightarrow{DB_2}=\begin{bmatrix}p_x+\frac{\sqrt{3}h}{2}n_x-\frac{1}{2}hl_x\\p_y+\frac{\sqrt{3}h}{2}n_y-\frac{1}{2}hl_y\\p_z+\frac{\sqrt{3}h}{2}n_z-\frac{1}{2}hl_z\end{bmatrix} \quad \overrightarrow{DB_3}=\begin{bmatrix}p_x-\frac{\sqrt{3}h}{2}n_x-\frac{1}{2}hl_x\\p_y-\frac{\sqrt{3}h}{2}n_y-\frac{1}{2}hl_y\\p_z-\frac{\sqrt{3}h}{2}n_z-\frac{1}{2}hl_z\end{bmatrix}. \tag{64}$$

In the RPS structure, each leg is connected to the fixed base by a revolute joint (A_1, A_2 or A_3) and to the moving platform by a spherical joint (B_1, B_2 or B_3). Therefore, each leg's motion is constrained in one of the following three planes, as can be written by observing equation (63):

$$(DB_1)_x = 0, \tag{65}$$

where, $(DB_1)_x$ and $(DB_1)_z$ are the *x* and *z* components of $\overrightarrow{DB_1}$

$$(DB_2)_x = -\sqrt{3}(DB_2)_z, \tag{66}$$

where, $(DB_2)_x$ and $(DB_2)_z$ are the *x* and *z* components of $\overrightarrow{DB_2}$

$$(DB_3)_x = \sqrt{3}(DB_3)_z, \tag{67}$$

where, $(DB_3)_x$ and $(DB_3)_z$ are the *x* and *z* components of $\overrightarrow{DB_3}$.

Substituting the *x* and *z* components of equation (64) into equations (65) to (67) provides,

$$p_x + hl_x = 0, \tag{68}$$

$$p_x + \frac{\sqrt{3}h}{2}n_x - \frac{1}{2}hl_x = -\sqrt{3}(p_z + \frac{\sqrt{3}h}{2}n_z - \frac{1}{2}hl_z), \tag{69}$$

$$p_x - \frac{\sqrt{3}h}{2}n_x - \frac{1}{2}hl_x = \sqrt{3}(p_z - \frac{\sqrt{3}h}{2}n_z - \frac{1}{2}hl_z). \tag{70}$$

The following two equations can be obtained from equations (68) to (70):

$$l_x = n_z \tag{71}$$

and

$$p_z = \frac{1}{2}h(l_z\text{-}n_x). \quad (72)$$

Appendix 2

Symbols used	Definitions	Note
$\boldsymbol{\alpha}$	Pitch or rotation about the x_T axis of the coordinate$x_t y_t z_t$.	See Figure 2.
$\boldsymbol{\beta}$	Yaw or rotation about the y_T axis of the coordinate$x_t y_t z_t$.	See Figure 2.
$\boldsymbol{u}$	Tip or the rotational motion of the RPS mechanism about the *x* axis of the *xyz* frame to orientate the moving platform with respect to *xyz*.	See section 3.4.1.
$\boldsymbol{v}$	Tilt or the rotational motion of the motor about the *y´* axis of the *x´y´z´* frame to orientate the rotating platform with respect to the *x´y´z´*.	See section 3.4.1.
$\boldsymbol{\delta_{x_{err}}}$ and $\boldsymbol{\delta_{z_{err}}}$	Translational error motions of the moving platform related to tip rotation *u*.	See section 3.4 and Figure 4.
$\boldsymbol{u_{err}}$	Rotational error motion of the moving platform related to the tip rotation *u*.	See section 3.4 and Figure 4.
$\boldsymbol{\delta_{x_{rad}}}$ and $\boldsymbol{\delta_{z_{rad}}}$	Translational error motions of the rotating platform related to the tilt rotation *v*.	See section 3.4 and Figure 4.
$\boldsymbol{\varepsilon_x}$ and $\boldsymbol{\varepsilon_z}$	Rotational error motions of the rotating platform related to the tilt rotation *v*.	See section 3.4 and Figure 4
$\boldsymbol{d_3}$	Offset of the target from the centroid of the moving platform in the *z* direction.	See Figure 2.
$\boldsymbol{h_5}$	Offset between the centroids of the moving and rotating platform in the *y* direction.	See Figure 2.
$\boldsymbol{h_6}$	Offset between the centroid of the rotating platform and the centre of the target interface wheel in the *y* direction.	See Figure 2.
$\boldsymbol{t_x}$, $\boldsymbol{t_y}$, $\boldsymbol{t_z}$	Coordinate position of the target *T* with respect to the reference coordinate $x_w y_w z_w$, placed at the centre of the target interface wheel.	See Figure 2.